

# Reduced N-Type $\text{Ca}^{2+}$ Channels in Atrioventricular Ganglion Neurons Are Involved in Ventricular Arrhythmogenesis

Dongze Zhang, MD; Huiyin Tu, PhD; Liang Cao, MD; Hong Zheng, MD; Robert L. Muelleman, MD; Michael C. Wadman, MD; Yu-Long Li, MD, PhD

**Background**—Attenuated cardiac vagal activity is associated with ventricular arrhythmogenesis and related mortality in patients with chronic heart failure. Our recent study has shown that expression of N-type  $\text{Ca}^{2+}$  channel  $\alpha$ -subunits ( $\text{Ca}_v2.2\text{-}\alpha$ ) and N-type  $\text{Ca}^{2+}$  currents are reduced in intracardiac ganglion neurons from rats with chronic heart failure. Rat intracardiac ganglia are divided into the atrioventricular ganglion (AVG) and sinoatrial ganglion. Ventricular myocardium receives projection of neuronal terminals only from the AVG. In this study we tested whether a decrease in N-type  $\text{Ca}^{2+}$  channels in AVG neurons contributes to ventricular arrhythmogenesis.

**Methods and Results**—Lentiviral  $\text{Ca}_v2.2\text{-}\alpha$  shRNA ( $2\ \mu\text{L}$ ,  $2 \times 10^7$  pfu/mL) or scrambled shRNA was in vivo transfected into rat AVG neurons. Nontransfected sham rats served as controls. Using real-time single-cell polymerase chain reaction and reverse-phase protein array, we found that in vivo transfection of  $\text{Ca}_v2.2\text{-}\alpha$  shRNA decreased expression of  $\text{Ca}_v2.2\text{-}\alpha$  mRNA and protein in rat AVG neurons. Whole-cell patch-clamp data showed that  $\text{Ca}_v2.2\text{-}\alpha$  shRNA reduced N-type  $\text{Ca}^{2+}$  currents and cell excitability in AVG neurons. The data from telemetry electrocardiographic recording demonstrated that 83% (5 out of 6) of conscious rats with  $\text{Ca}_v2.2\text{-}\alpha$  shRNA transfection had premature ventricular contractions ( $P < 0.05$  versus 0% of nontransfected sham rats or scrambled shRNA-transfected rats). Additionally, an index of susceptibility to ventricular arrhythmias, inducibility of ventricular arrhythmias evoked by programmed electrical stimulation, was higher in rats with  $\text{Ca}_v2.2\text{-}\alpha$  shRNA transfection compared with nontransfected sham rats and scrambled shRNA-transfected rats.

**Conclusions**—A decrease in N-type  $\text{Ca}^{2+}$  channels in AVG neurons attenuates vagal control of ventricular myocardium, thereby initiating ventricular arrhythmias. (*J Am Heart Assoc.* 2018;7:e007457. DOI: 10.1161/JAHA.117.007457.)

**Key Words:** autonomic nervous system • calcium channel • ECG • ganglia • parasympathetic • vagus nerve • ventricular arrhythmia

**M**alignant ventricular arrhythmia including ventricular tachycardia (VT) and ventricular fibrillation (VF) is a common complication in chronic heart failure (CHF) and accounts for nearly 50% to 60% of mortality in patients with CHF.<sup>1–6</sup> Cardiac autonomic dysfunction is a major feature of CHF, characterized by a sustained increase of sympathetic tone and withdrawal of cardiac vagal activity.<sup>7–9</sup> Much evidence has shown that this autonomic imbalance leads to

arrhythmogenesis and is associated with the high mortality of CHF.<sup>2,10,11</sup> The role of sympathetic hyperactivation in CHF is highlighted by a blockade of the sympathetic nervous system ( $\beta$ -adrenergic receptor blockers) as the key approach to the current therapy of CHF.<sup>12–14</sup> However, such pharmacological treatment is not ideal because the ability of  $\beta$ -adrenergic receptor blockers to affect cardiac vagal activity is limited,<sup>15</sup> and survival rates even when  $\beta$ -blockers are used are lower in CHF patients with depressed cardiac vagal activity than in CHF patients with normal cardiac vagal activity.<sup>16</sup> Although modulation of cardiac vagal activation as a potential therapy has received only limited attention, direct cardiac vagal nerve stimulation has been found to suppress ventricular tachyarrhythmia and to improve survival rates in CHF.<sup>17–19</sup> Therefore, exploring the mechanism(s) responsible for the impairment of cardiac vagal function can provide a new therapeutic strategy for eliminating ventricular tachyarrhythmia and reducing related mortality.

Cardiac vagal preganglionic fibers originate within the central nervous system at the brainstem (nucleus ambiguus,

From the Departments of Emergency Medicine (D.Z., H.T., L.C., R.L.M., M.C.W., Y.-L.L.), Cellular & Integrative Physiology (H.Z., Y.-L.L.), University of Nebraska Medical Center, Omaha, NE; Department of Cardiac surgery, Second Xiangya Hospital, Central South University, Changsha, China (L.C.).

**Correspondence to:** Yu-Long Li, MD, PhD, Department of Emergency Medicine, University of Nebraska Medical Center, 985850 Nebraska Medical Center, Omaha, NE 68198-5850. E-mail: yulongli@unmc.edu

Received August 21, 2017; accepted November 27, 2017.

© 2018 The Authors. Published on behalf of the American Heart Association, Inc., by Wiley. This is an open access article under the terms of the Creative Commons Attribution-NonCommercial-NoDerivs License, which permits use and distribution in any medium, provided the original work is properly cited, the use is non-commercial and no modifications or adaptations are made.

## Clinical Perspective

### What Is New?

- In vivo lentiviral transfection of Cav2.2- $\alpha$  shRNA into the rat atrioventricular ganglion decreases expression of Cav2.2- $\alpha$  mRNA and protein and N-type Ca<sup>2+</sup> currents in atrioventricular ganglion neurons.
- A decrease in N-type Ca<sup>2+</sup> channels in atrioventricular ganglion neurons blunts vagal control of the ventricle and initiates ventricular arrhythmogenesis.
- We provide direct evidence that blunted ventricular vagal activity triggers ventricular arrhythmogenesis.

### What Are the Clinical Implications?

- Withdrawal of cardiac vagal activity might be involved in occurrence of fatal ventricular arrhythmias in the chronic heart failure state.
- Improvement of the ventricular vagal activity might be an effective therapeutic strategy to limit malignant ventricular arrhythmias and cardiac sudden death in chronic heart failure.

nucleus tractus solitarius, and dorsal motor nucleus). The vagal preganglionic efferent extends to the intracardiac ganglia, located in cardiac fat pads, to form synapses with intracardiac ganglion neurons.<sup>20</sup> Intracardiac ganglion neurons provide local neural coordination independent of high brain centers.<sup>21</sup> Acetylcholine released from cardiac vagal efferent nerve terminals regulates cardiac function through binding to muscarinic acetylcholine receptors. It is known that Ca<sup>2+</sup> influx through voltage-gated Ca<sup>2+</sup> channels is a key trigger for acetylcholine release from nerve terminals.<sup>22</sup> Our recent study demonstrates that expression of N-type Ca<sup>2+</sup> channel  $\alpha$ -subunit (Cav2.2- $\alpha$ ) mRNA and protein is decreased in intracardiac ganglion neurons from CHF rats.<sup>23</sup> Rat intracardiac ganglia are divided into the sinoatrial ganglion and atrioventricular ganglion (AVG),<sup>24</sup> and the ventricle receives projection of nerve terminals only from the AVG.<sup>25</sup> In the present study, therefore, we used lentiviral Cav2.2- $\alpha$  shRNA to knock down expression of Cav2.2- $\alpha$  mRNA and protein in AVG neurons and tested the contribution of reduced N-type Ca<sup>2+</sup> channels in AVG neurons to ventricular arrhythmogenesis in conscious and anesthetized rats.

## Methods

All data, analytic methods, and study materials have been provided within the article.

## Experimental Animals

Male Sprague-Dawley rats (9-11 weeks of age) were used in this study. They were housed 2 per cage under controlled

temperature and humidity and a 12:12-hour dark-light cycle and were provided water and rat chow ad libitum. All experimental procedures were approved by the University of Nebraska Medical Center Institutional Animal Care and Use Committee and were carried out in accordance with the National Institutes of Health Guide for the Care and Use of Laboratory Animals.

## Microinjection of Lentiviral Cav2.2- $\alpha$ shRNA into the AVG

Under surgical anesthesia (2% isoflurane) and mechanical ventilation, rats were kept in right lateral recumbent position. A left posterolateral thoracotomy was done through the third left intercostal space on the back, and the left lung was moved aside to expose the AVG. There was a white color epicardial adipose pad at the junction of the inferior pulmonary veins and left atrium, which served as a marker for the virus microinjection because the AVG is located in this pad (Figure 1A). The heart beating was very weak at the junction of the inferior pulmonary veins and left atrium when the AVG was exposed under the left posterolateral thoracotomy, which ensured the success of the virus microinjection into the AVG. Under the microscope, lentiviral rat Cav2.2- $\alpha$  shRNA with phosphorylated green fluorescent protein (pGFP) or shRNA scramble control (2  $\mu$ L,  $2.0 \times 10^7$  pfu/mL, TL713159V and TR30021V, OriGene Technologies, Rockville, MD) was microinjected into the epicardial adipose pad by a glass micropipette connected to a WPI Nanoliter 2000 microinjector (Figure 1A). Scrambled shRNA was used to assess possible toxicity of lentivirus. After transfection, the chest was closed, and experiments were performed 1 week later to guarantee degradation of existing Cav2.2- $\alpha$  protein.

## Efficacy of Lentivirus Infection

Efficacy of the lentivirus infection was assessed by immunofluorescence staining. Briefly, isolated AVGs from 3 rats with transfection of lentiviral rat Cav2.2- $\alpha$  shRNA with pGFP were postfixed in 4% paraformaldehyde, followed by soaking of AVGs in 30% sucrose for 12 hours at 4°C for cryostat protection. AVGs were cut into 10- $\mu$ m-thick sections at -20°C and then mounted on precoated glass slides. AVG sections were incubated with 10% donkey serum for 1 hour, followed by incubation with goat anti-choline acetyltransferase antibody (a cholinergic neuronal marker; EMD Millipore, Billerica, MA) overnight at 4°C. Then AVG sections were incubated with fluorescence-conjugated secondary antibody (Invitrogen, Carlsbad, CA) for 1 hour at room temperature. AVG sections were examined under a Leica (Wetzlar, Germany) fluorescent microscope with corresponding filters for choline acetyltransferase (red color) and pGFP (green

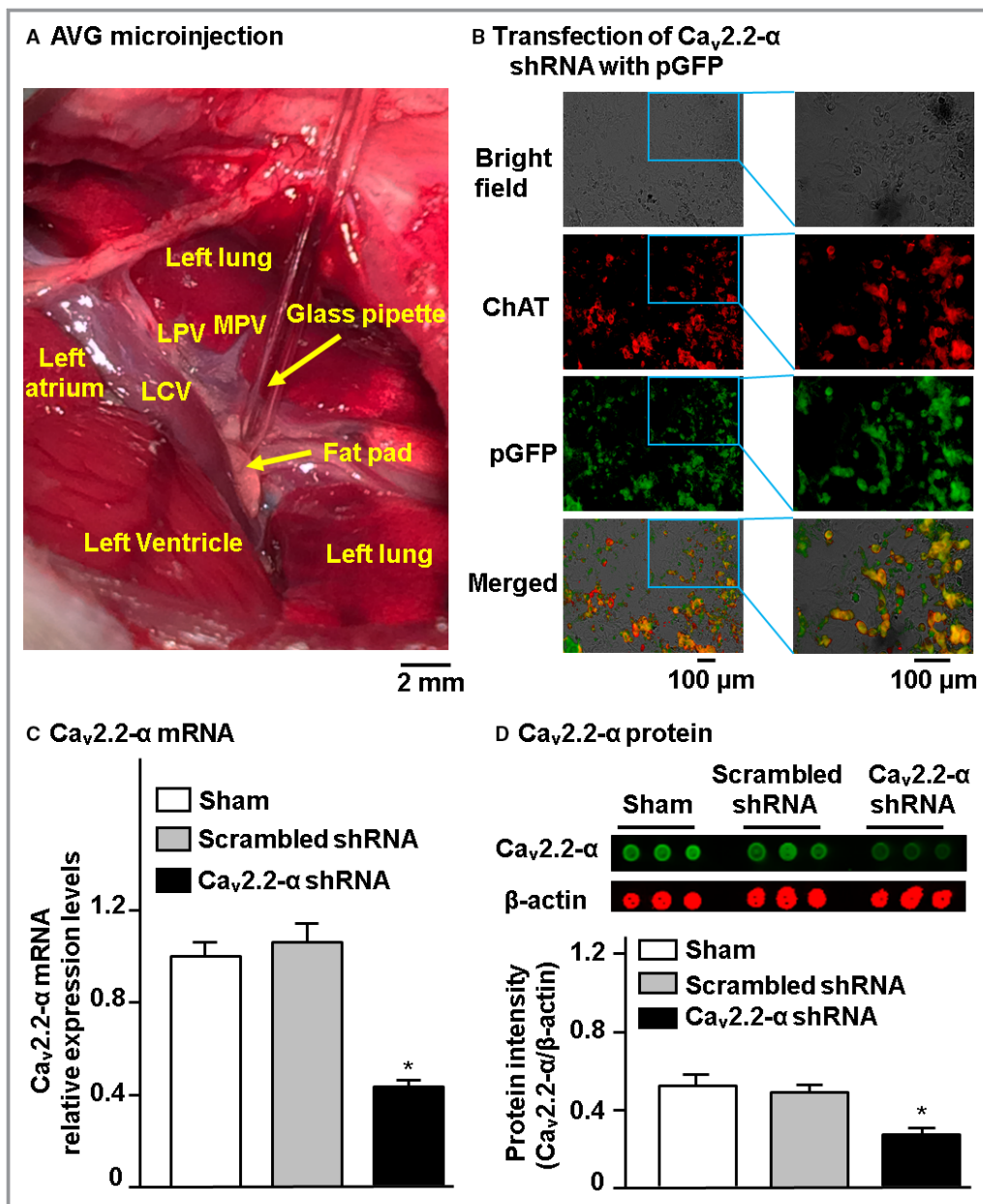


**Figure 1.** A, AVG microinjection under a rat left posterolateral thoracotomy. LCV indicates left cranial vein; LPV, left pulmonary vein; MPV, middle pulmonary vein. B, Expression of pGFP protein in rat cholinergic AVG neurons after in vivo lentiviral transfection of  $Ca_v2.2-\alpha$  shRNA with pGFP cDNA. C, Expression of  $Ca_v2.2-\alpha$  mRNA in Dil-labeled AVG neurons from all groups of rats, measured by single-cell real-time RT-PCR. N=20 neurons from 6 rats in each group. D, Expression of  $Ca_v2.2-\alpha$  protein in the AVG from all groups of rats, measured by reverse-phase protein microarray. N=3 rats in each group. Data are means $\pm$ SEM. Statistical significance in Figure 1C-D was determined by 1-way ANOVA with post hoc Dunnett test against the sham group. \* $P$ <0.05 vs sham. AVG indicates atrioventricular ganglion; ChAT, choline acetyltransferase; pGFP, phosphorylated green fluorescent protein; RT-PCR, reverse-transcription polymerase chain reaction.

color). The imaging was captured by a digital camera system. Figure 1B shows that microinjection of lentiviral rat  $Ca_v2.2-\alpha$  shRNA with pGFP into the AVG induced pGFP expression in almost all choline acetyltransferase-positive AVG neurons (n=3 rats), confirming the efficacy of virus infection and proper microinjection into the AVG.

### Labeling and Isolation of AVG Neurons

Although ventricular myocardium receives projection of nerve terminals only from the AVG,<sup>25</sup> it is possible that the AVG also innervates other parts of the heart. Therefore, we used a transported fluorescent dye (red color Dil) to retrograde-label

cardiac vagal neurons projecting to the ventricular myocardium. Rats were anesthetized with 2% isoflurane and artificially ventilated. After a left thoracotomy was performed to expose the heart, 8 injections (2  $\mu$ L Dil for each injection) were made subepicardially into the left ventricular myocardium using a glass micropipette connected to a WPI (Sarasota, FL) Nanoliter 2000 microinjector.<sup>23</sup> The surgical incision was closed, and terminal experiments were performed at least 3 days after labeling surgery because we found that 3 days are needed for dye diffusion to the neurons.<sup>23</sup> Dil-labeled AVG neurons (ventricular vagal neurons) were used to perform single-cell real-time reverse-transcription (RT) polymerase chain reaction (PCR) and whole-cell patch-clamp recording.

### ECG Transmitter Implantation and Electrocardiographic Recording

Each rat was anesthetized with 2% isoflurane (Butler Schein Animal Health, Dublin, OH). The skin was first shaved and sterilized. After laparotomy was performed at the linea alba (abdomen), the radiotelemetry ECG transmitter<sup>26</sup> (TRM54PB, Millar Instruments, Houston, TX) was placed into the abdominal cavity and secured to the abdominal wall at the best position for battery recharging and signal communication. In accordance with the Millar User Manual for ECG recording, bipolar electrodes were tunneled subcutaneously. The negative lead was secured in the upper sternal midline, and the positive lead was attached to the underlying tissue near the left side of the xiphoid process. In order to reduce the electrical noise during ECG recording, electrical leads were kept together and run alongside each other as far as practical. All incisions were sutured in 2 layers. ECG recording was performed after 1 week of recovery.

For ECG recording, rats were placed on a SmartPad receiver (Millar Instruments, Houston, TX). For quantification of ventricular arrhythmic events, 24-hour continuous ECG signals were acquired at room temperature from unrestrained, conscious rats. Real-time ECG signals were digitalized and analyzed by PowerLab 8/30 Data Acquisition System with LabChart 7 software and ECG analysis module (ADInstruments, Colorado Springs, CO). The number of premature ventricular contractions (PVCs) and cumulative duration of VT/VFs were counted manually during 24-hour continuous ECG recording. VT was defined as PVCs lasting  $\geq 4$  beats. VF was defined as rapid, irregular QRS complexes. QT and QTc intervals as well as dispersions (QTd and QTcd) were calculated from ECG recordings using LabChart 7 software.<sup>27</sup> A QTc interval was calculated by the Bazett formula ( $QT/\sqrt{RR}$ , where RR is the RR interval). As an index of the spatial dispersion of the ventricular repolarization, QTd and QTcd were calculated by equations:  $QTd = QT_{max} - QT_{min}$  and  $QTcd = QTc_{max} - QTc_{min}$ , where  $QT_{max}$

and  $QTc_{max}$  are the maximum QT interval and the maximum QTc interval;  $QT_{min}$  and  $QTc_{min}$  are the minimum QT interval and the minimum QTc interval.<sup>27</sup> The T-peak to T-end interval (Tpe), another marker of transmural dispersion of the ventricular repolarization, was calculated from ECG recordings to serve as an ECG marker of ventricular arrhythmia.<sup>28</sup>

### Measurement of Susceptibility to Ventricular Arrhythmias

Susceptibility to ventricular arrhythmias was measured as described previously.<sup>26</sup> On the day of the terminal experiment (1 day after radiotelemetry ECG recording), each rat was anesthetized (800 mg/kg urethane combined with 40 mg/kg  $\alpha$ -chloralose, intraperitoneally). The animal's trachea was cannulated to facilitate mechanical respiration. The animal's body temperature was maintained at 37°C with an Animal Temperature Controller (ATC 1000; World Precision Instruments, Sarasota, FL). Surface lead-II ECG was recorded using subcutaneous electrodes connected to a biological amplifier (AD Instruments, Colorado Springs, CO). A left thoracotomy was then performed in the fourth intercostal space. After the heart was visualized, the pericardium was carefully removed. A bipolar platinum stimulating electrode was placed on the right ventricle outflow tract for programmed electrical stimulation (PES). The PES was performed by a programmed electrical stimulator (Digital Pulse Generator 1831, WPI) and an isolator (A320R Isostim Stimulator, WPI). The pulse current output was set to a twice capture threshold and a 2-millisecond pulse width. To determine the ventricular effective refractory period, a train of 8 stimuli ( $8 \times S1$ ) at a 120-millisecond cycle length was applied, followed by an extra stimulus (S2). Starting at 90 milliseconds, the S1 to S2 interval was reduced in steps of 2 milliseconds until the ventricular effective refractory period was identified. Based on the ventricular effective refractory period, a programmed stimulation protocol combined by single (S2), double (S3), or triple extra stimulus (S4) after a train of 8 stimuli ( $8 \times S1$ ) was designed to induce ventricular tachyarrhythmias. The end point of ventricular pacing was induction of ventricular tachyarrhythmia. Ventricular tachyarrhythmia was considered noninducible when the PES induced either no ventricular premature beats or self-terminated ventricular premature beats  $< 6$ . Ventricular tachyarrhythmia was considered as nonsustained when it lasted  $\leq 15$  beats and sustained when it lasted  $> 15$  beats before spontaneously terminating.

Inducibility of ventricular tachyarrhythmia was quantified by a quotient of ventricular arrhythmic scores: 0, noninducible preparations; 1, nonsustained tachyarrhythmias induced with 3 extra stimuli; 2, sustained tachyarrhythmias induced with 3 extra stimuli; 3, nonsustained tachyarrhythmias induced with 2 extra stimuli; 4, sustained tachyarrhythmias induced with 2

extra stimuli; 5, nonsustained tachyarrhythmias induced with 1 extra stimulus; 6, sustained tachyarrhythmias induced with 1 extra stimulus; 7, tachyarrhythmias induced during a train of 8 stimuli ( $8 \times S_1$ ) at a basic cycle length of 120 milliseconds; 8, the heart stopped before the PES.

### Measurement of Hemodynamics and Vagal Control of Ventricular Function

After the susceptibility to ventricular arrhythmias had been detected, the left femoral artery was cannulated with a polyethylene-50 catheter for measurement of blood pressure and heart rate.<sup>26</sup> A Millar pressure transducer (SPR 524; Millar Instruments, Houston, TX) was slowly inserted into the right carotid artery and carefully advanced to the left ventricle for measurement of left ventricular pressure and the maximum rate of left ventricular pressure rise. Hemodynamic data were recorded by powerLab 8/30 Data Acquisition System with LabChart 7 software (ADInstruments, Colorado Springs, CO). Then, bilateral cervical vagal nerves, cervical sympathetic nerves, and aortic depressor nerves were isolated and transected to avoid influence of the arterial baroreflex. Because we found that the response of left ventricular systolic pressure (LVSP) to left vagal efferent nerve stimulation was markedly stronger than that to right vagal efferent nerve stimulation, the peripheral end of the left vagal nerve was placed on a bipolar stimulating electrode for vagal efferent nerve stimulation. Left vagal efferent nerve stimulation was applied by a Grass S9 stimulator (Grass Instruments, Quincy, MA) with 10 seconds of constant-frequency stimulation (0.1 milliseconds pulse duration and intensity of 7.5 V, 1–100 Hz). As the index of vagal control of ventricular function, changes of LVSP and maximum rate of left ventricular pressure rise in response to different frequencies of left efferent vagal stimulation were recorded by a PowerLab 8/30 data acquisition system with LabChart 7 software (AD Instruments, Colorado Springs, CO).

### Isolation of AVG Neurons and Single-Cell Real-Time RT-PCR

After in-vivo experiments were performed, the AVG, located in a white epicardial adipose pad at the junction of inferior pulmonary veins and left atrium, was exposed. AVG neurons were isolated by a 2-step enzymatic digestion protocol, as described previously.<sup>23,29</sup> Isolated AVG was placed in ice-cold modified Tyrode solution (mmol/L): 140 NaCl, 5 KCl, 10 HEPES, and 5 glucose. The AVG was minced with microscissors and incubated with a modified Tyrode solution containing 0.1% collagenase and 0.1% trypsin for 30 minutes at 37°C. The tissue was then transferred to a modified Tyrode solution containing 0.2% collagenase and 0.5% bovine serum albumin

for 30 minutes of incubation at 37°C. The isolated neurons were cultured at 37°C in a humidified atmosphere of 95% air–5% CO<sub>2</sub> for single-cell real-time RT-PCR and patch-clamp experiments.

Single-cell real-time RT-PCR was performed as described previously.<sup>23</sup> Briefly, isolated AVG neurons were loaded in a chamber with regular extracellular solution (in mmol/L): 137 NaCl, 5.4 KCl, 1 MgCl<sub>2</sub>, 2 CaCl<sub>2</sub>, 10 HEPES, 10 glucose with pH 7.4. DiI-labeled AVG neurons (ventricular vagal neurons) were used for single-cell real-time RT-PCR. A patch-clamp pipette (1–3 MΩ resistance) was used to break the membrane of single neuronal cell. Under the suction condition, cell and pipette content were expelled into a 0.2-mL PCR tube containing mRNA preserving reagents and then mixed with RT reaction buffer. RT was performed at 42°C for 30 minutes, and the cDNA was then stored at –80°C. The primers (Table 1) were based on the cDNA sequences of RPL19 (housekeeping gene) and Ca<sub>v</sub>2.2-α. PCR reaction was performed in a 25-μL volume containing 12.5 μL iQ Syber Green Supermix (Bio-Rad, Hercules, CA), 200 nmol/L (in the first round) or 300 nmol/L (in the second round) of each primer. The cDNA was amplified by real-time quantitative PCR with an ABI StepOnePlus Real-Time PCR System. For quantification, Ca<sub>v</sub>2.2-α gene was normalized to housekeeping gene RPL19. The data were analyzed by the 2<sup>–ΔΔCt</sup> method.<sup>30</sup>

### Reverse-Phase Protein Microarray for Protein Expression

Due to the limitation of small AVG samples (1–2 mg wet weight), we could not detect the expression of Ca<sub>v</sub>2.2-α protein using regular Western blot analyses and instead employed a modified reverse-phase protein microarray, which is highly sensitive and needs about 1 μg protein.<sup>31</sup> Briefly, total protein concentration of AVG samples was determined using a bicinchoninic acid protein assay kit (Pierce, Rockford, IL). Fifty nanoliters of each protein sample was loaded onto nitrocellulose-coated glass slides by an 8-pin arrayer. After protein samples were sequentially incubated with primary antibodies (rabbit anti-Ca<sub>v</sub>2.2-α antibody and mouse anti-β-

**Table 1.** Primer Sequences

Gene Accession	Primer Name	Primer Sequence (5'–3')
NM0147141	Ca <sub>v</sub> 2.2-forward	TCCTAGCCAGGTGTCCCATC
	Ca <sub>v</sub> 2.2-reverse	CTTTCCAGGGACCTCTGCTTC
	Ca <sub>v</sub> 2.2-internal	CCACCACCACCGCTGCCACCG
NM031103	RPL19-forward	CTGAAGGTCAAAGGGAATGTGTTT
	RPL19-reverse	TTCGTGCTTCTTGGTCTTAGAC
	RPL19-internal	TGCGAGCTCAGCCTGGTCAGCC

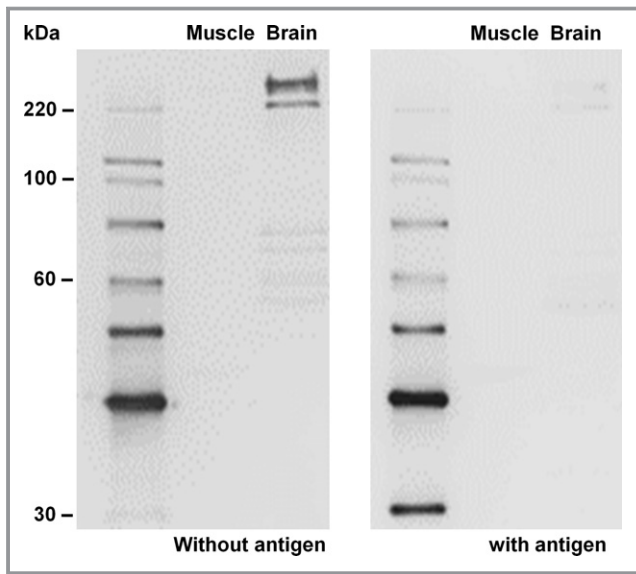


**Figure 2.** Western blot image for expression of Cav2.2- $\alpha$  protein in rat brain and gastrocnemius muscle with or without peptide antigen. Rat brain was used as Cav2.2- $\alpha$ -positive tissue, and gastrocnemius muscle was used as Cav2.2- $\alpha$ -negative tissue.

actin antibody) and LI-COR fluorescence-conjugated secondary antibodies (IRDye 800CW goat anti-rabbit IgG and IRDye 680LT goat anti-mouse IgG), the protein signals were scanned with a LI-COR Odyssey IR imaging system (LI-COR, Lincoln, NE). Before reverse-phase protein microarray was performed, Western blot analysis was used to validate target specificity of Cav2.2- $\alpha$  antibody by blocking with antigen peptide to confirm elimination of specific signal and testing against tissues known to express (rat brain) or not express Cav2.2- $\alpha$  protein (rat gastrocnemius muscle) (Figure 2).

### Western Blot Analysis for Validation of Target Specificity of Cav2.2- $\alpha$ Antibody

The rat brain was used as Cav2.2- $\alpha$ -positive tissue, and gastrocnemius muscle was used as Cav2.2- $\alpha$ -negative tissue.<sup>32,33</sup> The fresh tissues were homogenized with a lysing buffer (10 mmol/L Tris, 1 mmol/L EDTA, 150 mmol/L NaCl, 1% SDS, 1 mmol/L PMSF; pH 7.4) plus protease inhibitor cocktail (100  $\mu$ L/mL; Sigma, St. Louis, MO). After centrifugation at 12 000g for 20 minutes at 4°C, the protein concentration in the supernatant was determined using a bicinchoninic acid protein assay kit (Pierce, Rockford, IL). The protein samples were mixed with the same volume of the loading buffer and heated for 5 minutes at 100°C. Equal amounts of protein samples (40  $\mu$ g/well) were loaded and then separated on a 9% sodium dodecyl sulfate polyacrylamide gel. Proteins of these samples were electrophoretically transferred at 200 mA for 3 hours onto polyvinylidene fluoride membrane (EMD Millipore,

Billerica, MA). The membrane was blocked with 5% nonfat milk in Tris-buffered saline-tween 20 (20 mmol/L Tris, 150 mmol/L NaCl, 0.05% [v/v] Tween-20) for 1 hour. Then the membrane was probed with rabbit primary antibody against Cav2.2- $\alpha$  (1:800; Alomone Labs, Jerusalem, Israel) or with a mixture of anti-Cav2.2- $\alpha$  antibody and peptide antigen (preincubated 10  $\mu$ g of peptide antigen with 10  $\mu$ g of anti-Cav2.2- $\alpha$  antibody for 1 hour at room temperature) overnight at 4°C. After washing, the membrane was incubated for 1 hour with peroxidase-conjugated appropriate secondary antibody (Pierce Chemical, Rockford, IL). The signal was detected using enhanced chemiluminescence substrate (Pierce Chemical), and all bands were analyzed using a UVP bioimaging system (UVP, Upland, CA). Anti-Cav2.2- $\alpha$  antibody recognized proteins of 250 and 220 kDa, 2 size forms of Cav2.2- $\alpha$  subunit in the rat brain,<sup>34,35</sup> but not in the rat skeletal muscle. All bands disappeared when antigenic peptide was preincubated (Figure 2).

### Whole-Cell Patch-Clamp Recording for Ca<sup>2+</sup> Currents and Action Potentials

After isolation of AVG neurons (see above), voltage-gated Ca<sup>2+</sup> currents and action potentials were recorded only in Dil-labeled AVG neurons (ventricular vagal neurons) by the whole-cell patch-clamp technique using an Axopatch 200B patch-clamp amplifier (Molecular Devices, Sunnyvale, CA).<sup>23</sup>

In voltage-clamp experiments, resistance of the patch pipette was 4 to 6 M $\Omega$  when the pipette was filled with the following solution (in mmol/L): 120 CsCl, 1 CaCl<sub>2</sub>, 40 HEPES, 11 EGTA, 4 MgATP, 0.3 Tris-GTP, 14 creatine phosphate, and 0.1 leupeptin (pH 7.3; 305 mosmol/kg). The extracellular solution consisted of (in mmol/L): 140 TEA-Cl, 5 BaCl<sub>2</sub>, 1 MgCl<sub>2</sub>, 10 HEPES, 0.001 TTX, 2 4-AP, and 10 glucose (pH 7.4; 310 mosmol/kg). Series resistance of 5 to 13 M $\Omega$  was electronically compensated at 30% to 80%. The junction potential was calculated to be +7.9 mV using the P-clamp 10.2 program (Molecular Devices, Sunnyvale, CA), and all values of membrane potential given throughout were corrected using this value. Current traces were sampled at 10 kHz and filtered at 5 kHz. The holding potential was -80 mV, and current-voltage relationships were elicited by 5-mV step increments to potentials between -60 and 60 mV for 500 milliseconds. N-type Ca<sup>2+</sup> currents were obtained by subtracting the Ca<sup>2+</sup> currents under treatment with  $\omega$ -conotoxin GVIA from total Ca<sup>2+</sup> currents. Based on the previous study, the concentration of  $\omega$ -conotoxin GVIA (1  $\mu$ mol/L, a specific N-type Ca<sup>2+</sup> channel blocker) used in the present study is a saturating concentration for inhibiting N-type Ca<sup>2+</sup> channels.<sup>23,36</sup> Peak currents were measured for each test potential, and current density was calculated by dividing peak current by cell membrane capacitance.

In current-clamp experiments action potentials were elicited by a ramp current injection of 0 to 100 pA, and frequency of action potentials was measured in a 1-second current clamp. The patch-pipette solution was composed of (in mmol/L): 105 K-aspartate, 20 KCl, 1 CaCl<sub>2</sub>, 5 MgATP, 10 HEPES, 10 EGTA, and 25 glucose (pH 7.2; 320 mosmol/kg). The bath solution was composed of (in mmol/L): 140 NaCl, 5.4 KCl, 0.5 MgCl<sub>2</sub>, 2.5 CaCl<sub>2</sub>, 5.5 HEPES, 11 glucose, and 10 sucrose (pH 7.4; 330 mosmol/kg). Junction potential was calculated to be +12.3 mV, and membrane potential was corrected using this value. The P-clamp 10.2 program (Molecular Devices, Sunnyvale, CA) was used for data acquisition and analysis. All experiments were done at room temperature (22–24°C).

### Statistical Analysis

All data are presented as means±SEM. SigmaPlot 12 (Systat Software, Chicago, IL) was used for data analysis. We analyzed the normal distribution of the data using the Kolmogorov-Smirnov test and found that statistical analyses for the normal distribution of the data are passed in all parameters. Statistical significance was determined by a Fisher exact test for incidence of ventricular arrhythmias because some cells have fewer than 5 expected observations. Statistical significance was determined by 1-way ANOVA with post hoc Dunnett test against the sham group for most of the parameters. Statistical significance in some experiments was determined by 1-way repeated-measures ANOVA with post hoc Dunnett test against the sham group. Statistical significance was determined by paired t-test for comparison between before and after treatments. Because of the heterogeneity among the dissociated neurons from 1 animal, we used neuron numbers to do statistical analyses for Ca<sub>v</sub>2.2-α mRNA, N-type Ca<sup>2+</sup> currents, and action potentials. Statistical significance was accepted when *P*<0.05.

## Results

### Efficacy of Lentiviral Ca<sub>v</sub>2.2-α shRNA

To verify efficacy of lentiviral Ca<sub>v</sub>2.2-α shRNA transfected into the AVG, expression of Ca<sub>v</sub>2.2-α mRNA and protein in AVG neurons was measured in all groups of rats. We initially confirmed that there was expression of Ca<sub>v</sub>2.2-α mRNA and protein in AVG neurons from sham rats. In vivo lentiviral transfection of Ca<sub>v</sub>2.2-α shRNA into the AVG reduced expression of Ca<sub>v</sub>2.2-α mRNA and protein in AVG neurons, which were about 43% and 52% of Ca<sub>v</sub>2.2-α mRNA and protein levels seen in sham AVG neurons, respectively (Figure 1C and 1D). However, shRNA scramble control had no effect on expression of Ca<sub>v</sub>2.2-α mRNA and protein in AVG neurons (Figure 1C and 1D).

### Influence of Ca<sub>v</sub>2.2-α shRNA on N-Type Ca<sup>2+</sup> Currents and Cell Excitability in AVG Neurons

Voltage-gated Ca<sup>2+</sup> currents and action potentials in Dil-labeled AVG neurons (ventricular vagal neurons) were recorded by whole-cell patch-clamp technique. A specific N-type Ca<sup>2+</sup> channel blocker (1 μmol/L ω-conotoxin GVIA) was used to separate N-type Ca<sup>2+</sup> currents from total Ca<sup>2+</sup> currents. N-type Ca<sup>2+</sup> currents were obtained by subtracting Ca<sup>2+</sup> currents under treatment with ω-conotoxin GVIA from total Ca<sup>2+</sup> currents (Figure 3Aa). Ca<sub>v</sub>2.2-α shRNA but not shRNA scramble control decreased N-type Ca<sup>2+</sup> currents in ventricular vagal neurons (Figure 3Aa through 3Ac). Ca<sub>v</sub>2.2-α shRNA also reduced frequency of action potentials (a parameter of the cell excitability) in ventricular vagal neurons (Figure 3Ba and 3Bb). However, there were no significant differences in resting membrane potential, input resistance, and cell membrane capacitance in ventricular vagal neurons from all groups of rats (Table 2).

### Ca<sub>v</sub>2.2-α shRNA Attenuated Vagal Control of the Ventricle

We hypothesized that attenuated ventricular vagal activity through in vivo transfection of Ca<sub>v</sub>2.2-α shRNA into AVG neurons could be linked to ventricular arrhythmogenesis. Activation of the vagal efferent nerve results in a negative inotropic effect in the ventricle, which serves as an index of ventricular vagal function.<sup>37</sup> Ca<sub>v</sub>2.2-α shRNA transfection into AVG neurons significantly blunted changes of the LVSP and maximum rate of left ventricular pressure rise in response to vagal efferent nerve stimulation, compared with sham rats (Figure 4). However, shRNA scramble control did not show any effect on vagal control of the ventricle. Additionally, transfection of Ca<sub>v</sub>2.2-α shRNA into AVG neurons increased basal LVSP with the absence of heart-rate changes (Table 3), which further confirmed that transfection of Ca<sub>v</sub>2.2-α shRNA into AVG neurons only blunted ventricular vagal activity and did not affect sinoatrial vagal activity.

### Effect of Ca<sub>v</sub>2.2-α shRNA on Susceptibility to Ventricular Arrhythmias in Anesthetized Rats

Figure 5 shows the effect of Ca<sub>v</sub>2.2-α shRNA on the susceptibility to ventricular arrhythmias in anesthetized rats (Figure 5). A PES protocol was performed to induce ventricular arrhythmias in anesthetized rats, and an inducibility quotient was used to evaluate the susceptibility to ventricular arrhythmias. Ventricular arrhythmias were not induced by S<sub>1</sub>S<sub>2</sub>S<sub>3</sub>S<sub>4</sub> programmed stimulation, and the inducibility quotient of ventricular arrhythmias was 0 in sham rats (Figure 5). After in vivo transfection of Ca<sub>v</sub>2.2-α shRNA into AVG neurons, 83.3% (5/6) of the rats had PES-induced ventricular arrhythmias, and the inducibility quotient of ventricular arrhythmias was 1.97±0.49 (Figure 5; *P*<0.05 versus

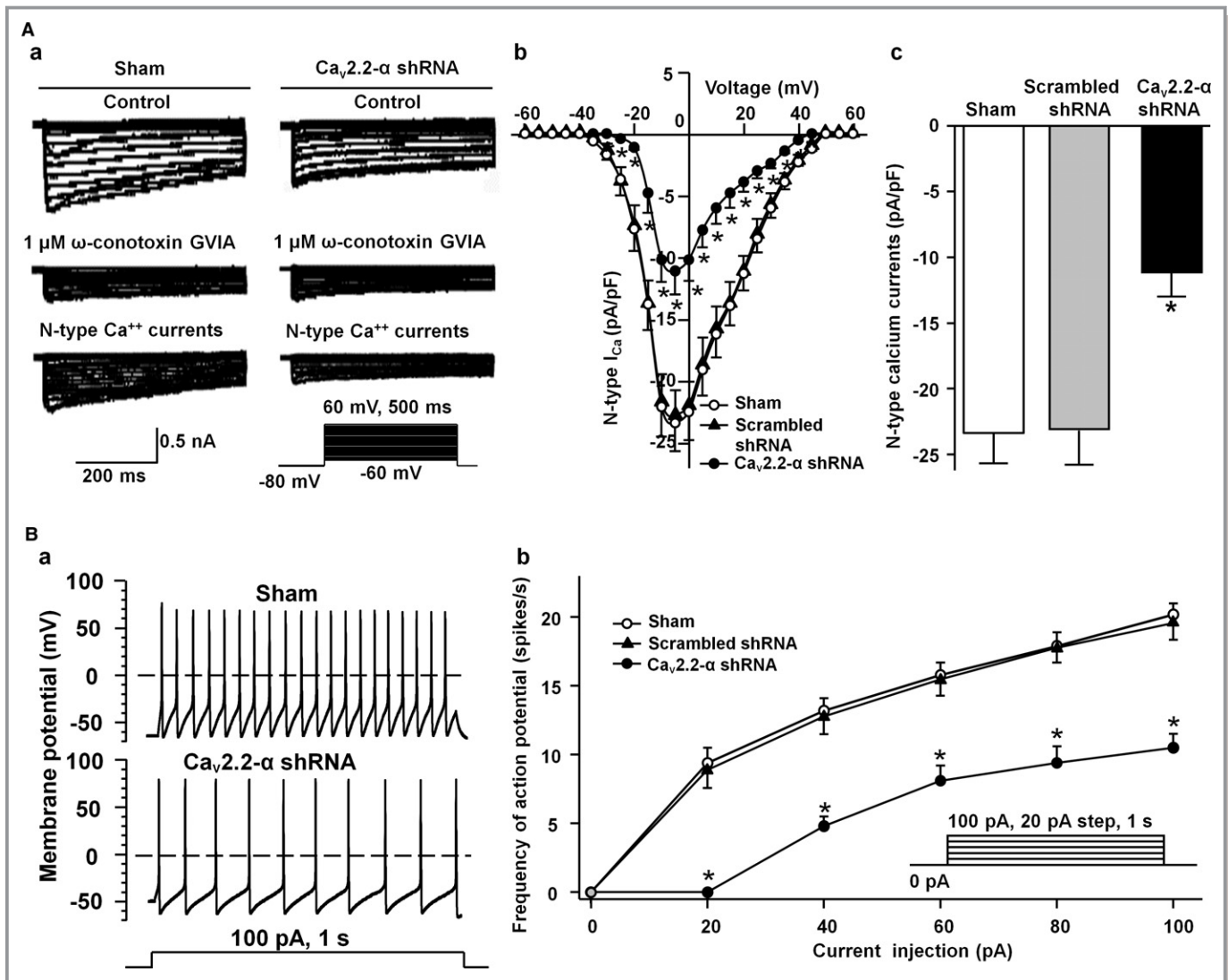


**Figure 3.** A, original recording of  $\text{Ca}^{2+}$  currents (a), current-voltage curve (b), and mean data (c, at 5-mV test voltage) of N-type  $\text{Ca}^{2+}$  currents in DiI-labeled AVG neurons from all groups of rats. B, original recording of action potentials (a) and frequency of action potentials (b) in DiI-labeled AVG neurons from all groups of rats.  $\omega$ -Conotoxin GVIA is a specific N-type  $\text{Ca}^{2+}$  channel blocker. Data are means  $\pm$  SEM from  $n=8$  neurons from 6 rats in each group. Statistical significance was determined by 1-way repeated-measures ANOVA with post hoc Dunnett test against the sham group in (Ab and Bb), and 1-way ANOVA with post hoc Dunnett test against the sham group in 3Ac, respectively.  $*P < 0.05$  vs sham. AVG indicates atrioventricular ganglion.

sham rats). However, there was nonoccurrence of PES-induced ventricular arrhythmias in rats with transfection of shRNA scramble control (Figure 5).

### Effect of $\text{Ca}_v2.2\text{-}\alpha$ shRNA on Spontaneous Ventricular Arrhythmias and ECG Parameters in Conscious Rats

Spontaneous ventricular arrhythmias and ECG parameters in conscious rats were monitored by radiotelemetry ECG recording (Figures 6 and 7). There was nonoccurrence of spontaneous ventricular arrhythmias in sham rats (0/6 of the

rats, Figure 6). After in vivo transfection of  $\text{Ca}_v2.2\text{-}\alpha$  shRNA into AVG neurons, 83.3% (5/6) of the rats had PVCs, and the number of spontaneous PVCs was  $10 \pm 4$  beats/h (Figure 6;  $P < 0.05$  versus sham rats). In vivo transfection of shRNA scramble control into AVG neurons did not induce spontaneous ventricular arrhythmias (Figure 6).

Simultaneously, in vivo transfection of  $\text{Ca}_v2.2\text{-}\alpha$  shRNA into AVG neurons increased the QT interval, QTc interval, QT<sub>d</sub>, QTc<sub>d</sub>, and Tpe, compared with sham rats or before treatment with  $\text{Ca}_v2.2\text{-}\alpha$  shRNA (Figure 7;  $P < 0.05$ ). However, scrambled shRNA did not affect these arrhythmia-related ECG parameters (Figure 7).

**Table 2.** Electrophysiological Changes on Cell Membrane Properties in DiI-Labeled AVG Neurons From All Groups of Rats

	Sham	Scrambled shRNA	Ca <sub>v</sub> 2.2-α shRNA
RMP, mV	60.1±1.1	60.4±1.3	59.9±1.2
R <sub>i</sub> , GΩ	0.82±0.08	0.79±0.09	0.81±0.08
C <sub>m</sub> , pF	32.4±1.7	32.6±1.4	32.2±1.4

Data are means±SEM; n=8 neurons from 6 rats in each group. Statistical significance was determined by 1-way ANOVA with post hoc Dunnett test against the sham group. AVG indicates atrioventricular ganglion; C<sub>m</sub>, cell membrane capacitance; R<sub>i</sub>, input resistance; RMP, resting membrane potential.

## Discussion

In the present study we tested the influence of reduced N-type Ca<sup>2+</sup> channels in ventricular vagal neurons located in the AVG on ventricular arrhythmogenesis and documented the following findings. First, *in vivo* transfection of Ca<sub>v</sub>2.2-α shRNA into AVG neurons decreased expression and ion currents of N-type Ca<sup>2+</sup> channels and cell excitability in ventricular vagal neurons. Second, *in vivo* transfection of Ca<sub>v</sub>2.2-α shRNA into AVG neurons attenuated vagal control of the ventricle. Third, *in vivo* transfection of Ca<sub>v</sub>2.2-α shRNA into AVG neurons increased the susceptibility to ventricular arrhythmias in anesthetized rats. Finally, *in vivo* transfection of Ca<sub>v</sub>2.2-α shRNA into AVG neurons induced occurrence of PVCs and changes of arrhythmia-related ECG parameters including prolongation of QT, QT<sub>c</sub>, and T<sub>pe</sub> and increase in QT<sub>d</sub> and QT<sub>c,d</sub> in conscious rats. These findings suggest that a decrease in N-type Ca<sup>2+</sup> channels in ventricular vagal neurons blunts ventricular vagal activity and triggers ventricular arrhythmogenesis.

Like a natural yin-yang pair, the sympathetic and parasympathetic nervous systems play an important regulatory role in heart functions including cardiac electrophysiology and cardiac muscle contraction. In particular, a sustained increase of sympathetic activity and a marked decrease of parasympathetic tone are used as distinctive hallmarks of CHF.<sup>7-9</sup> Thus far, most of the studies used the analysis of heart-rate variability and arterial baroreflex sensitivity to evaluate cardiac sympathetic and parasympathetic autonomic activity in physiological and pathophysiological conditions.<sup>38</sup> Although traditional teaching has stated that cardiac vagal postganglionic nerves regulate the heart through slowing sinus rate and atrioventricular conduction, with little influence on ventricles, and ventricular vagal innervation is considered to be sparse,<sup>18,39</sup> newer histological techniques have challenged this traditional principle and affirmed dense vagal innervation in the ventricle from all species.<sup>18,40-43</sup> Recent studies have demonstrated that functionally significant parasympathetic control of ventricular contractile function and excitability

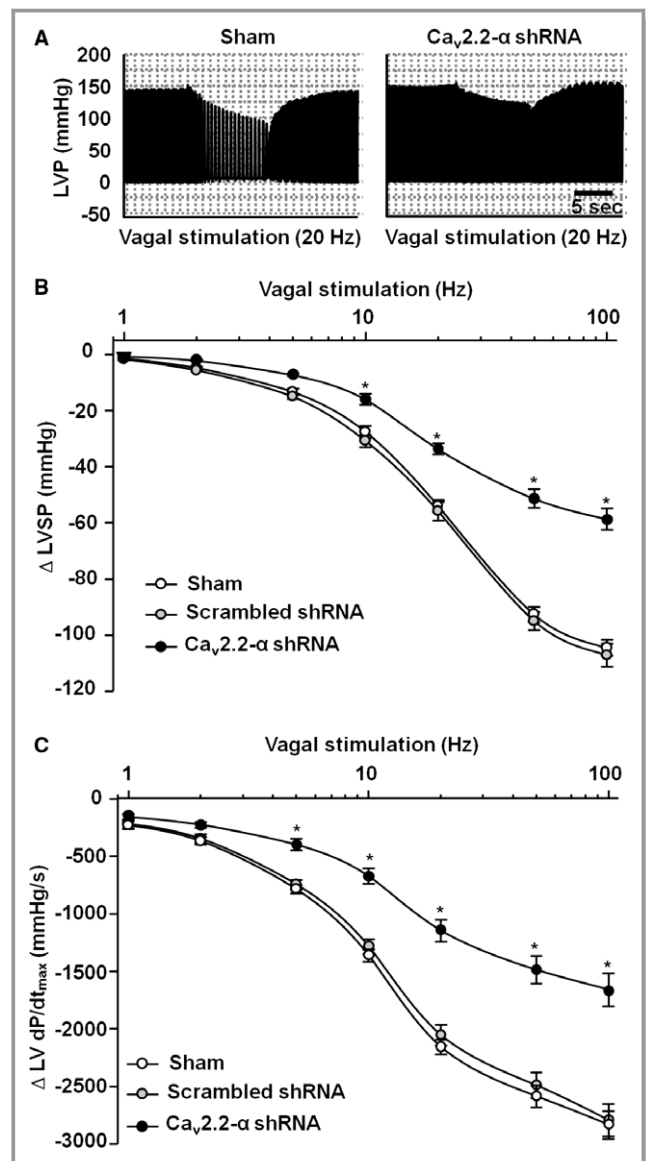


**Figure 4.** Representative tracings of the LVP (A), and mean data showing changes of the LVSP (B) and LV dP/dt<sub>max</sub> (C) in response to different frequency of left vagal efferent nerve stimulation in all groups of anesthetized rats. LV indicates left ventricle; LV dP/dt<sub>max</sub>, peak rate of change of LVP; LVP, left ventricular pressure; LVSP, left ventricular systolic pressure. Data are means±SEM; n=6 rats in each group. Statistical significance was determined by 1-way repeated-measures with post hoc Dunnett test against the sham group (B and C). \**P*<0.05 vs sham.

exists in rats, and vagal preganglionic neurons of the dorsal motor nucleus contribute to the vagal control of ventricular contractility and excitability.<sup>44,45</sup> Therefore, directly examining ventricular vagal activity is very useful to assess the vagal modulation of ventricular arrhythmia and contractile dysfunction. Cardiac vagal postganglionic neurons are located in the intracardiac ganglia. Rat intracardiac ganglia are divided into the sinoatrial ganglion and the AVG.<sup>24</sup> The ventricular myocardium only receives the projection of nerve terminals

**Table 3.** Basal Hemodynamic Characteristics in All Groups of Anesthetized Rats

	Sham (n=6)	Scrambled shRNA (n=6)	Ca <sub>v</sub> 2.2-α shRNA (n=12)
Body weight, g	358.4±5.6	356.2±7.4	359.4±5.3
MBP, mm Hg	102.6±3.6	103.7±3.5	103.5±2.7
HR, bpm	349±5	351±7	354±5.2
LVSP, mm Hg	120.6±3.1	121.5±3.6	144.9±3.2*
LVEDP, mm Hg	1.9±0.3	2.0±0.4	2.0±0.3
LV dP/dt <sub>max</sub> , mm Hg/s	5918.4±204.4	5999.3±225.3	6472.7±187.8

Mean blood pressure (MBP), heart rate (HR), left ventricular systolic pressure (LVSP), left ventricular end-diastolic pressure (LVEDP), and the maximum rate of left ventricular pressure rise (LV dP/dt<sub>max</sub>) were measured under anesthetized condition on the day of the terminal experiment. Data are means±SEM. Statistical significance was determined by 1-way ANOVA with post hoc Dunnett test against the sham group.

\**P*<0.05 vs sham.

from the AVG.<sup>25</sup> In our present study we measured the left ventricular pressure and vagal efferent nerve stimulation-induced negative inotropic response in the left ventricle; the

latter serves as an index of ventricular vagal activity.<sup>37</sup> In vivo transfection of Ca<sub>v</sub>2.2-α shRNA into AVG neurons increased basal LVSP with the absence of heart-rate changes in anesthetized rats (Table 3). In vivo transfection of Ca<sub>v</sub>2.2-α shRNA into AVG neurons also attenuated changes of the LVSP and maximum rate of left ventricular pressure rise in response to left vagal efferent nerve stimulation (Figure 4). These results not only confirmed that ventricular contractile function is directly regulated by ventricular vagal postganglionic neurons located in the AVG but also clarified that ventricular vagal activity is attenuated by a decrease in N-type Ca<sup>2+</sup> channels in ventricular vagal postganglionic neurons.

Fatal ventricular arrhythmias including VT and VF are associated with high mortality in patients with CHF.<sup>1,3-5</sup> Based on the fact that the occurrence of fatal ventricular arrhythmias is accompanied by a marked decrease of parasympathetic activity in CHF, some studies demonstrate that decreased parasympathetic activity is correlated with malignant ventricular arrhythmogenesis in the CHF state.<sup>11,46-48</sup> Recent studies have also found that the parasympathetic activation induced by vagal nerve stimulation prevents fatal

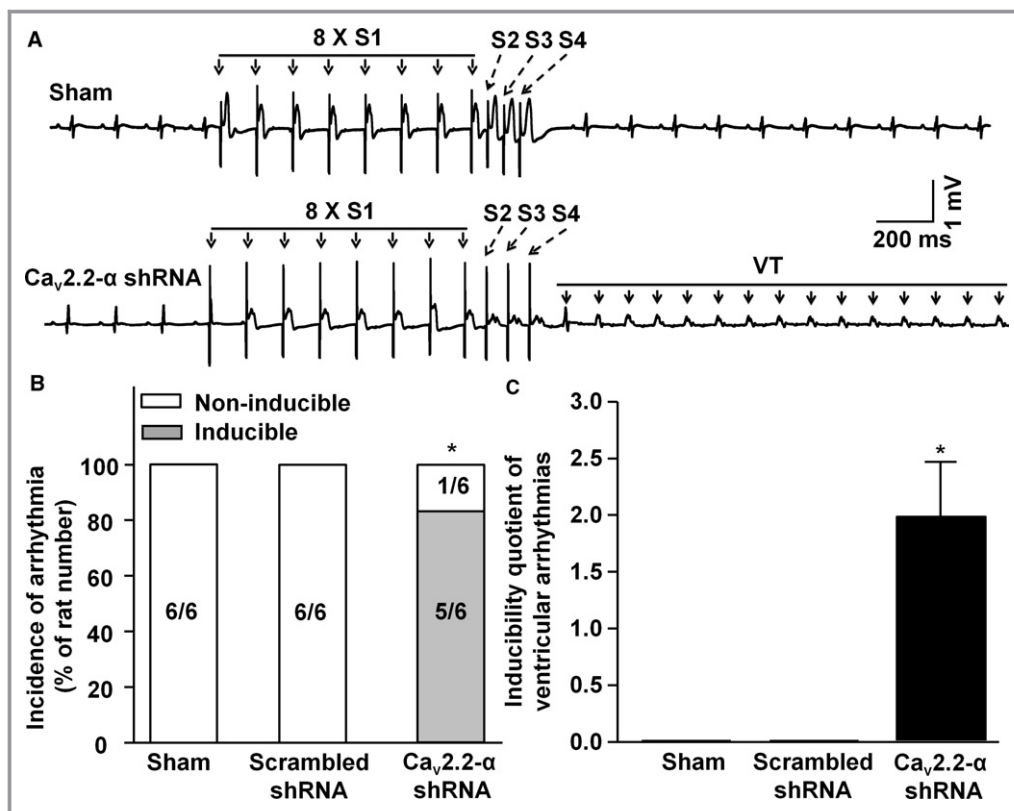


**Figure 5.** A, Raw data for induction of ventricular arrhythmias evoked by programmed electrical stimulation (S1-4). B and C, Incidence and inducibility quotient of ventricular arrhythmias in all groups of rats. Data are means±SEM; n=6 rats in each group. Statistical significance was determined by Fisher exact test (B) or 1-way ANOVA with post hoc Dunnett test against the sham group (C), respectively. \**P*<0.05 vs sham.

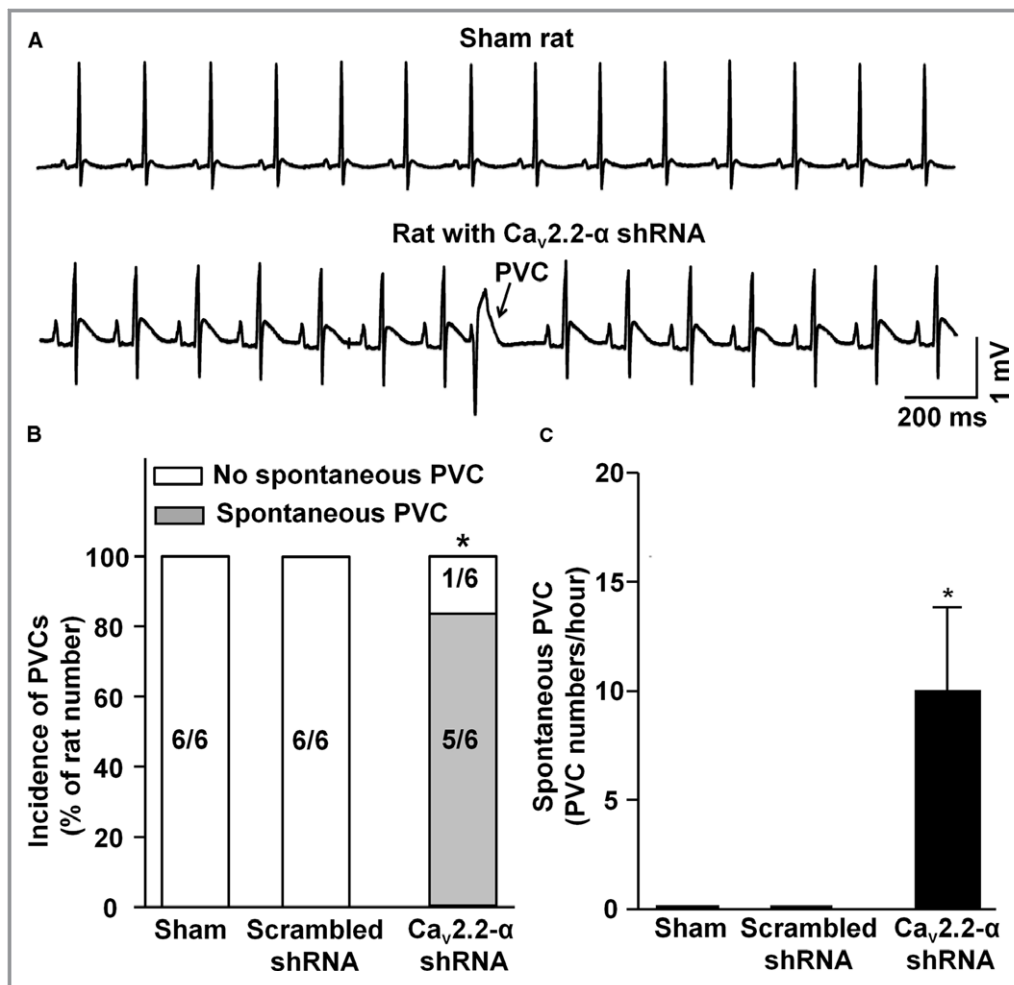


**Figure 6.** Representative data of ECG recording (A), mean data for incidence of ventricular arrhythmia (B), and the number of premature ventricular contraction (PVC) in all groups of conscious rats. Data are means $\pm$ SEM; n=6 rats in each group. Statistical significance was determined by Fisher exact test (B) or by 1-way ANOVA with post hoc Dunnett test against the sham group (C). \* $P$ <0.05 vs sham.

ventricular arrhythmias and improves survival rates in animal CHF models.<sup>17-19</sup> However, there is no direct evidence to clarify the role of decreased parasympathetic activity in ventricular arrhythmogenesis and how decreased parasympathetic activity links to ventricular arrhythmogenesis in CHF due to the coexistence of multiple factors in the CHF state (such as sympathetic overactivation, ventricular morphological changes, and others). In the present study in vivo transfection of Ca<sub>v</sub>2.2-α shRNA into AVG neurons decreased expression and ion currents of N-type Ca<sup>2+</sup> channels and cell excitability in ventricular vagal neurons (Figures 1 and 3) and blunted the ventricular vagal activity (Figure 4) as well as increased the susceptibility to ventricular arrhythmias of anesthetized rats (Figure 5). More importantly, ECG data obtained from radiotelemetry recording demonstrated that in vivo transfection of Ca<sub>v</sub>2.2-α shRNA into AVG neurons not only increased the QT interval, QTc interval, QTd, QTcd, and Tpe but also induced a spontaneous ventricular

tachyarrhythmia in conscious rats (Figures 6 and 7). It has been found that prolongation of the QT and QTc intervals, increase of the QTd and QTcd (a marker of spatial heterogeneity of ventricular repolarization), and prolonged Tpe (a marker of transmural dispersion of ventricular repolarization) are associated with increased risk of malignant ventricular arrhythmias and sudden cardiac death.<sup>49-52</sup> The results in the present study provide direct evidence that blunted ventricular vagal activity increases the susceptibility to ventricular arrhythmias and induces ventricular arrhythmias.

Our recent study has demonstrated that the occurrence of lethal ventricular arrhythmias is accompanied by reduced N-type Ca<sup>2+</sup> currents in AVG neurons and blunted ventricular vagal activity in coronary artery ligation-induced CHF rats.<sup>26</sup> In the present study, although in vivo transfection of Ca<sub>v</sub>2.2-α shRNA into AVG neurons significantly decreased expression and ion currents of N-type Ca<sup>2+</sup> channels in ventricular vagal

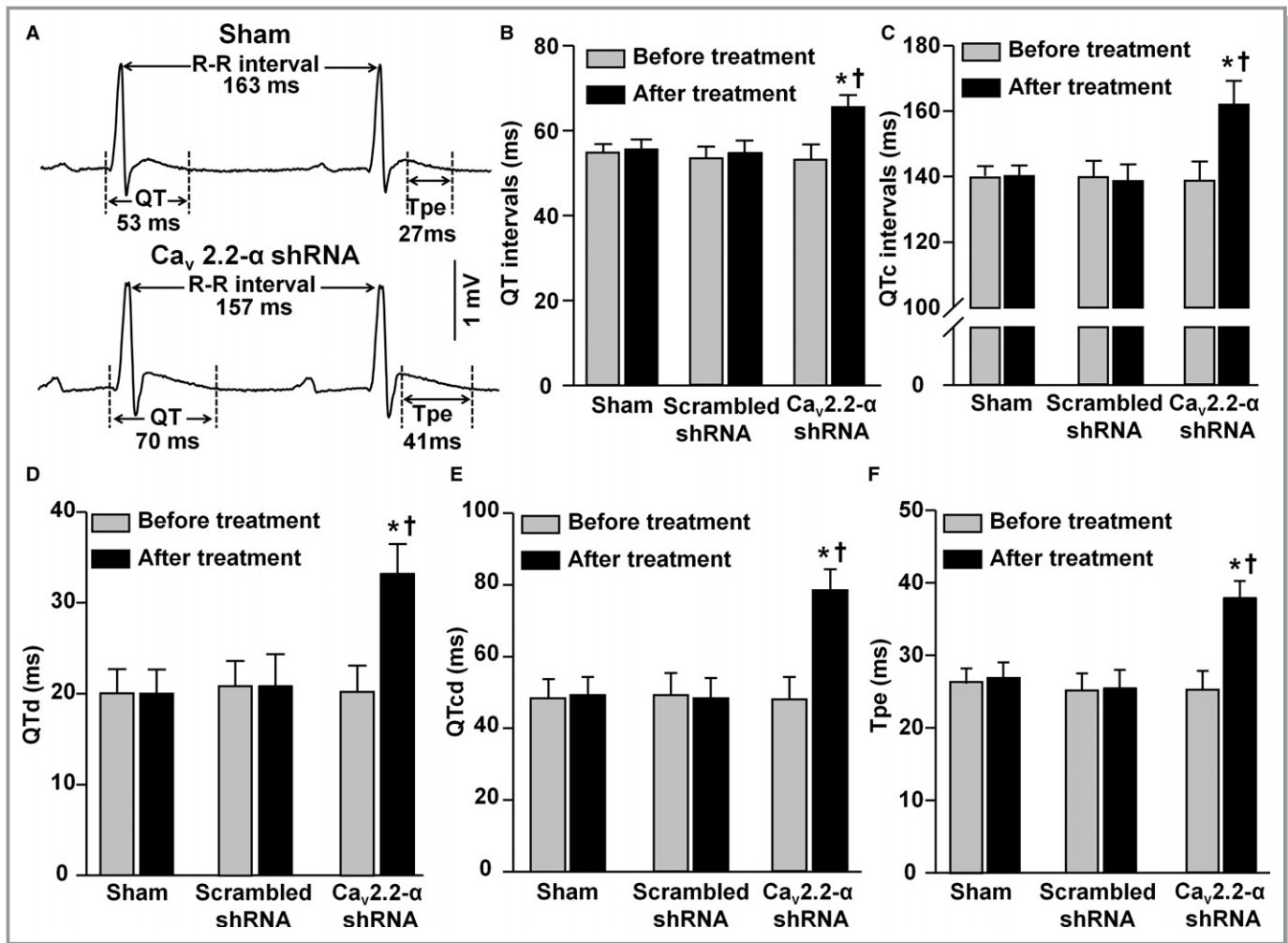


**Figure 7.** A, Representative signal of electrocardiographic recordings illustrating QT intervals and T-peak to T-end interval (Tpe) in sham and Cav2.2- $\alpha$  shRNA transfected rats. B through F, Mean data for QT intervals, QTc intervals, QT dispersions (QTd), QTc dispersions (QTcd), and Tpe in all groups of conscious rats. Data are means $\pm$ SEM; n=6 rats in each group. Statistical significance was determined by 1-way ANOVA with post hoc Dunnett test against the sham group for comparison among multiple groups or by paired t test for comparison between before and after treatments, respectively. \* $P$ <0.05 vs sham; † $P$ <0.05 vs before treatment.

neurons and blunted ventricular vagal activity, it merely induced spontaneous PVCs but not lethal ventricular arrhythmias such as VT/VF in conscious rats. In general, the combination of proarrhythmic substrates and triggers is necessary to initiate lethal ventricular arrhythmias under the CHF state. Besides blunted ventricular vagal activity, therefore, other determinants of ventricular arrhythmias such as myocardial infarction and sympathetic overactivation are the prerequisite factors for fatal ventricular arrhythmogenesis.

Because of the limitation of small AVG samples (1–2 mg wet weight), we could not detect expression of Ca<sub>v</sub>2.2- $\alpha$  mRNA and protein using regular real-time RT-PCR and Western blot analyses and instead employed single-cell real-time RT-PCR and modified reverse-phase protein microarray. Before performing reverse-phase protein microarray, therefore, we used the rat brain as a Ca<sub>v</sub>2.2- $\alpha$ -positive sample and the gastrocnemius muscle as a Ca<sub>v</sub>2.2- $\alpha$ -negative sample to

evaluate target specificity of Ca<sub>v</sub>2.2- $\alpha$  antibody (Figure 2). Additionally, we do realize a possible limitation of small animals for extrapolating the findings obtained in this study to humans, although the rat has contributed markedly to assessment of the pathophysiology and treatment of CHF and to the advancement of clinical care.<sup>53–55</sup> Large animals could be an appropriate alternative for translational experiments. However, the lack of genetic and molecular tools (including a viral vector carrying large-animal genes or shRNAs, and antibodies for large animals) does not allow us to use large animals for these experiments in this study.

A hallmark of CHF, withdrawal of cardiac vagal activity, is associated with ventricular arrhythmogenesis, yet sites and mechanisms involved in abnormal cardiac vagal activity remain unclear. Although our recent study demonstrates that the decrease of N-type Ca<sup>2+</sup> currents in AVG neurons correlates with occurrence of ventricular arrhythmias in

CHF rats,<sup>26</sup> we could not clarify whether the occurrence of ventricular arrhythmia in CHF rats is totally or partially due to neuronal remodeling of AVN neurons. This is because these experiments were performed with both coronary artery ligation-induced CHF and other determinants of ventricular arrhythmias, such as CHF-induced changes of ventricular myocytes themselves. Our current study decreases N-type Ca<sup>2+</sup> channels in AVN neurons and ventricular vagal activity in sham rats without changing the above factors. Therefore, this current study provides direct evidence that blunted ventricular vagal activity is a determinant of ventricular arrhythmogenesis to increase the susceptibility to ventricular arrhythmias and initiate ventricular arrhythmias as a trigger. Improvement of the ventricular vagal activity might be an effective therapeutic strategy to limit malignant ventricular arrhythmias and cardiac sudden death in patients with CHF.

## Sources of Funding

This study was supported by the American Heart Association (Grant-in-Aid 15GRANT24970002 to Li), and National Heart, Lung, and Blood Institute (grant R01HL-137832A to Li).

## Disclosures

None.

## References

- Carson P, Anand I, O'Connor C, Jaski B, Steinberg J, Lwin A, Lindenfeld J, Ghali J, Barnett JH, Feldman AM, Bristow MR. Mode of death in advanced heart failure: the Comparison of Medical, Pacing, and Defibrillation Therapies in Heart Failure (COMPANION) trial. *J Am Coll Cardiol*. 2005;46:2329–2334.
- Cygankiewicz I, Zareba W, Vazquez R, Vallverdu M, Gonzalez-Juanatey JR, Valdes M, Almendral J, Cinca J, Caminal P, de Luna AB. Heart rate turbulence predicts all-cause mortality and sudden death in congestive heart failure patients. *Heart Rhythm*. 2008;5:1095–1102.
- Huikuri HV, Castellanos A, Myerburg RJ. Sudden death due to cardiac arrhythmias. *N Engl J Med*. 2001;345:1473–1482.
- Podrid PJ, Fogel RI, Fuchs TT. Ventricular arrhythmia in congestive heart failure. *Am J Cardiol*. 1992;69:82G–95G.
- Singh BN. Significance and control of cardiac arrhythmias in patients with congestive cardiac failure. *Heart Fail Rev*. 2002;7:285–300.
- Thompson BS. Sudden cardiac death and heart failure. *AACN Adv Crit Care*. 2009;20:356–365.
- Porter TR, Eckberg DL, Fritsch JM, Rea RF, Beightol LA, Schmedtje JF Jr, Mohanty PK. Autonomic pathophysiology in heart failure patients. Sympathetic-cholinergic interrelations. *J Clin Invest*. 1990;85:1362–1371.
- Saul JP, Arai Y, Berger RD, Lilly LS, Colucci WS, Cohen RJ. Assessment of autonomic regulation in chronic congestive heart failure by heart rate spectral analysis. *Am J Cardiol*. 1988;61:1292–1299.
- Schwartz PJ, De Ferrari GM. Sympathetic-parasympathetic interaction in health and disease: abnormalities and relevance in heart failure. *Heart Fail Rev*. 2011;16:101–107.
- Boogers MJ, Veltman CE, Bax JJ. Cardiac autonomic nervous system in heart failure: imaging technique and clinical implications. *Curr Cardiol Rev*. 2011;7:35–42.
- Hauptman PJ, Schwartz PJ, Gold MR, Borggrefe M, Van Veldhuisen DJ, Starling RC, Mann DL. Rationale and study design of the increase of vagal tone in heart failure study: INOVATE-HF. *Am Heart J*. 2012;163:954–962.
- Gheorghide M, Colucci WS, Swedberg K. Beta-blockers in chronic heart failure. *Circulation*. 2003;107:1570–1575.
- Nevezorov R, Porath A, Henkin Y, Kobal SL, Jotkowitz A, Novack V. Effect of beta blocker therapy on survival of patients with heart failure and preserved systolic function following hospitalization with acute decompensated heart failure. *Eur J Intern Med*. 2012;23:374–378.
- Packer M, Bristow MR, Cohn JN, Colucci WS, Fowler MB, Gilbert EM, Shusterman NH. The effect of carvedilol on morbidity and mortality in patients with chronic heart failure. U.S. Carvedilol Heart Failure Study Group. *N Engl J Med*. 1996;334:1349–1355.
- Desai MY, Watanabe MA, Laddu AA, Hauptman PJ. Pharmacologic modulation of parasympathetic activity in heart failure. *Heart Fail Rev*. 2011;16:179–193.
- La Rovere MT, Pinna GD, Maestri R, Robbi E, Caporotondi A, Guazzotti G, Sleight P, Febo O. Prognostic implications of baroreflex sensitivity in heart failure patients in the beta-blocking era. *J Am Coll Cardiol*. 2009;53:193–199.
- Brack KE, Coote JH, Ng GA. Vagus nerve stimulation protects against ventricular fibrillation independent of muscarinic receptor activation. *Cardiovasc Res*. 2011;91:437–446.
- Brack KE, Winter J, Ng GA. Mechanisms underlying the autonomic modulation of ventricular fibrillation initiation-tentative prophylactic properties of vagus nerve stimulation on malignant arrhythmias in heart failure. *Heart Fail Rev*. 2013;18:389–408.
- Zheng C, Li M, Inagaki M, Kawada T, Sunagawa K, Sugimachi M. Vagal stimulation markedly suppresses arrhythmias in conscious rats with chronic heart failure after myocardial infarction. *Conf Proc IEEE Eng Med Biol Soc*. 2005;7:7072–7075.
- Olshansky B, Sabbah HN, Hauptman PJ, Colucci WS. Parasympathetic nervous system and heart failure: pathophysiology and potential implications for therapy. *Circulation*. 2008;118:863–871.
- Verrier RL, Antzelevitch C. Autonomic aspects of arrhythmogenesis: the enduring and the new. *Curr Opin Cardiol*. 2004;19:2–11.
- Akiyama T, Yamazaki T. Adrenergic inhibition of endogenous acetylcholine release on postganglionic cardiac vagal nerve terminals. *Cardiovasc Res*. 2000;46:531–538.
- Tu H, Liu J, Zhang D, Zheng H, Patel KP, Cornish KG, Wang WZ, Muelleman RL, Li YL. Heart failure-induced changes of voltage-gated Ca<sup>2+</sup> channels and cell excitability in rat cardiac postganglionic neurons. *Am J Physiol Cell Physiol*. 2014;306:C132–C142.
- Sampaio KN, Mauad H, Spyer KM, Ford TW. Differential chronotropic and dromotropic responses to focal stimulation of cardiac vagal ganglia in the rat. *Exp Physiol*. 2003;88:315–327.
- Pardini BJ, Patel KP, Schmid PG, Lund DD. Location, distribution and projections of intracardiac ganglion cells in the rat. *J Auton Nerv Syst*. 1987;20:91–101.
- Zhang D, Tu H, Wang C, Cao L, Muelleman RL, Wadman MC, Li YL. Correlation of ventricular arrhythmogenesis with neuronal remodeling of cardiac postganglionic parasympathetic neurons in the late stage of heart failure after myocardial infarction. *Front Neurosci*. 2017;11:252.
- Costa EC, Goncalves AA, Areas MA, Morgabel RG. Effects of metformin on QT and QTc interval dispersion of diabetic rats. *Arq Bras Cardiol*. 2008;90:232–238.
- Yagishita D, Chui RW, Yamakawa K, Rajendran PS, Ajjola OA, Nakamura K, So EL, Mahajan A, Shivkumar K, Vaseghi M. Sympathetic nerve stimulation, not circulating norepinephrine, modulates T-peak to T-end interval by increasing global dispersion of repolarization. *Circ Arrhythm Electrophysiol*. 2015;8:174–185.
- Liu J, Tu H, Zheng H, Zhang L, Tran TP, Muelleman RL, Li YL. Alterations of calcium channels and cell excitability in intracardiac ganglion neurons from type 2 diabetic rats. *Am J Physiol Cell Physiol*. 2012;302:C1119–C1127.
- Livak KJ, Schmittgen TD. Analysis of relative gene expression data using real-time quantitative PCR and the 2(-Delta Delta C(T)) Method. *Methods*. 2001;25:402–408.
- Gallagher RL, Silvestri A, Petricoin EF III, Liotta LA, Espina V. Reverse phase protein microarrays: fluorometric and colorimetric detection. *Methods Mol Biol*. 2011;723:275–301.
- Ertel EA, Campbell KP, Harpold MM, Hofmann F, Mori Y, Perez-Reyes E, Schwartz A, Snutch TP, Tanabe T, Birnbaumer L, Tsien RW, Catterall WA. Nomenclature of voltage-gated calcium channels. *Neuron*. 2000;25:533–535.
- Trimmer JS, Rhodes KJ. Localization of voltage-gated ion channels in mammalian brain. *Annu Rev Physiol*. 2004;66:477–519.
- Westenbroek RE, Hell JW, Warner C, Dubel SJ, Snutch TP, Catterall WA. Biochemical properties and subcellular distribution of an N-type calcium channel alpha 1 subunit. *Neuron*. 1992;9:1099–1115.

35. Hell JW, Appleyard SM, Yokoyama CT, Warner C, Catterall WA. Differential phosphorylation of two size forms of the N-type calcium channel alpha 1 subunit which have different COOH termini. *J Biol Chem*. 1994;269:7390–7396.
36. Jeong SW, Wurster RD. Calcium channel currents in acutely dissociated intracardiac neurons from adult rats. *J Neurophysiol*. 1997;77:1769–1778.
37. Lewis ME, Al-Khalidi AH, Bonser RS, Clutton-Brock T, Morton D, Paterson D, Townend JN, Coote JH. Vagus nerve stimulation decreases left ventricular contractility in vivo in the human and pig heart. *J Physiol*. 2001;534:547–552.
38. Shen MJ, Zipes DP. Role of the autonomic nervous system in modulating cardiac arrhythmias. *Circ Res*. 2014;114:1004–1021.
39. Sroka K. On the genesis of myocardial ischemia. *Z Kardiol*. 2004;93:768–783.
40. Kawano H, Okada R, Yano K. Histological study on the distribution of autonomic nerves in the human heart. *Heart Vessels*. 2003;18:32–39.
41. Rysevaite K, Saburkina I, Pauziene N, Vaitkevicius R, Noujaim SF, Jalife J, Pauza DH. Immunohistochemical characterization of the intrinsic cardiac neural plexus in whole-mount mouse heart preparations. *Heart Rhythm*. 2011;8:731–738.
42. Ulphani JS, Cain JH, Inderyas F, Gordon D, Gikas PV, Shade G, Mayor D, Arora R, Kadish AH, Goldberger JJ. Quantitative analysis of parasympathetic innervation of the porcine heart. *Heart Rhythm*. 2010;7:1113–1119.
43. Xu XL, Zang WJ, Lu J, Kang XQ, Li M, Yu XJ. Effects of carvedilol on M2 receptors and cholinesterase-positive nerves in adriamycin-induced rat failing heart. *Auton Neurosci*. 2006;130:6–16.
44. Machhada A, Ang R, Ackland GL, Ninkina N, Buchman VL, Lythgoe MF, Trapp S, Tinker A, Marina N, Gourine AV. Control of ventricular excitability by neurons of the dorsal motor nucleus of the vagus nerve. *Heart Rhythm*. 2015;12:2285–2293.
45. Machhada A, Marina N, Korsak A, Stuckey DJ, Lythgoe MF, Gourine AV. Origins of the vagal drive controlling left ventricular contractility. *J Physiol*. 2016;594:4017–4030.
46. Dibner-Dunlap ME, Smith ML, Kinugawa T, Thames MD. Enalaprilat augments arterial and cardiopulmonary baroreflex control of sympathetic nerve activity in patients with heart failure. *J Am Coll Cardiol*. 1996;27:358–364.
47. Nolan J, Batin PD, Andrews R, Lindsay SJ, Brooksby P, Mullen M, Baig W, Flapan AD, Cowley A, Prescott RJ, Neilson JM, Fox KA. Prospective study of heart rate variability and mortality in chronic heart failure: results of the United Kingdom heart failure evaluation and assessment of risk trial (UK-heart). *Circulation*. 1998;98:1510–1516.
48. Schwartz PJ, Vanoli E, Stramba-Badiale M, De Ferrari GM, Billman GE, Foreman RD. Autonomic mechanisms and sudden death. New insights from analysis of baroreceptor reflexes in conscious dogs with and without a myocardial infarction. *Circulation*. 1988;78:969–979.
49. Chugh SS, Reinier K, Singh T, Uy-Evanado A, Socoteanu C, Peters D, Mariani R, Gunson K, Jui J. Determinants of prolonged QT interval and their contribution to sudden death risk in coronary artery disease: the Oregon Sudden Unexpected Death Study. *Circulation*. 2009;119:663–670.
50. Morin DP, Saad MN, Shams OF, Owen JS, Xue JQ, Abi-Samra FM, Khatib S, Nelson-Twakor OS, Milani RV. Relationships between the T-peak to T-end interval, ventricular tachyarrhythmia, and death in left ventricular systolic dysfunction. *Europace*. 2012;14:1172–1179.
51. Panikkath R, Reinier K, Uy-Evanado A, Teodorescu C, Hattenhauer J, Mariani R, Gunson K, Jui J, Chugh SS. Prolonged Tpeak-to-tend interval on the resting ECG is associated with increased risk of sudden cardiac death. *Circ Arrhythm Electrophysiol*. 2011;4:441–447.
52. Straus SM, Kors JA, De Bruin ML, van der Hooft CS, Hofman A, Heeringa J, Deckers JW, Kingma JH, Sturkenboom MC, Stricker BH, Witteman JC. Prolonged QTc interval and risk of sudden cardiac death in a population of older adults. *J Am Coll Cardiol*. 2006;47:362–367.
53. Tucci PJ. Pathophysiological characteristics of the post-myocardial infarction heart failure model in rats. *Arq Bras Cardiol*. 2011;96:420–424.
54. Klocke R, Tian W, Kuhlmann MT, Nikol S. Surgical animal models of heart failure related to coronary heart disease. *Cardiovasc Res*. 2007;74:29–38.
55. Houser SR, Margulies KB, Murphy AM, Spinale FG, Francis GS, Prabhu SD, Rockman HA, Kass DA, Molkenin JD, Sussman MA, Koch WJ. Animal models of heart failure: a scientific statement from the American Heart Association. *Circ Res*. 2012;111:131–150.